Search for power-efficient wide-range reversible resistance modulation of VO$_2$ single crystals

To cite this article: Bertina Fisher *et al* 2019 *J. Phys. D: Appl. Phys.* **52** 385302

View the article online for updates and enhancements.

IOP ebooks™

Bringing you innovative digital publishing with leading voices to create your essential collection of books in STEM research.

Start exploring the collection - download the first chapter of every title for free.

Search for power-efficient wide-range reversible resistance modulation of VO$_2$ single crystals

Bertina Fisher[1,3]**, Larisa Patlagan**[1] **and Lior Kornblum**[2]

[1] Department of Physics, Technion—Israel Institute of Technology, Haifa 32000-03, Israel
[2] Andrew and Erna Viterbi Department of Electrical Engineering, Technion—Israel Institute of Technology, Haifa 32000-03, Israel

E-mail: phr06bf@physics.technion.ac.il

Abstract

The abrupt metal insulator transition in VO$_2$ is attracting considerable interest from both fundamental and applicative angles. We report on DC I–V characteristics measured on VO$_2$ single crystals in the two-probe configuration at several ambient temperatures below the insulator–metal (I–M) transition. The insulator-mixed-metal-insulator transition is induced by Joule heating above ambient temperature in the range of negative differential resistivity (NDR). In this range the stability of $I(V)$ is governed by the load resistance R$_L$. Steady state $I(V)$ is obtained for $R_L > |dV/dI|_{max}$ in the NDR regime. For $R_L < |dV/dI|_{max}$ there is switching between initial and final steady states associated with peaks in the Joule power, that are higher the lower R_L is. The peaks caused by steep switching are superfluous and damaging the samples. On the other hand, the large R_L needed for steady state is the main power consumer in the circuit at high currents. The present work is motivated by the need to avoid damaging switching in the NDR regime while reducing the power consumption in the circuit. Large resistance modulation can be obtained under steady state conditions with reduced power consumption by increasing the ambient temperature of the device above room temperature. Under steady state conditions, the transition to the mixed metal-insulator state is smooth and is followed closely by appearance of sliding domains.

Keywords: vanadium dioxide, metal-insulator transitions, negative differential resistance

S Supplementary material for this article is available online

(Some figures may appear in colour only in the online journal)

1. Introduction

Due to the outstanding insulator to metal transition (IMT) of VO$_2$ ($T_{IMT} = 340$ K, resistance jump of up to five orders of magnitude in single crystals accompanied by large changes in its structural and optical properties), this material has persisted for decades as a candidate for many potential applications [1], the most recent of which is for a new generation of electronics, electro-optics [2–11] and neuromorphic computing [12]. At the same time, recent studies continue to unveil fascinating mechanisms for these electronic features [13–15]. The insulator–metal (I–M) switching, whether induced thermally, optically or by an electric current is complex and induces a variety of mixed metal–insulator states and non-uniform stresses that produce mechanical degradation [16]. Most of the investigations are focused on thin films which are more robust than VO$_2$ single crystals. Here we report on switching induced by an electric current in single crystals. The results obtained here for the cleaner and sharper I–M switching can

[3] Author to whom any correspondence should be addressed.

J. Phys. D: Appl. Phys. **52** (2019) 385302

B Fisher *et al*

serve as guides for the design of thin film devices, as well as for freestanding nanocrystal applications. Under an applied voltage at ambient temperature, the resistance drops due to Joule heating, the voltage reaches a maximum (V_{max}) and a current controlled negative differential resistivity (CC-NDR) regime sets on. The mixed I–M phase appears within the NDR regime. The stability of $I(V)$ in this regime is governed by the magnitude of the load resistance (R_L) in series with the sample; I–V is stable for $R_L \geqslant |dV/dI|_{max}$—the absolute value of the steepest slope of $V(I)$ in the NDR regime [17]. For lower R_L, portions of the NDR regime are unstable and $I(V)$ switches from the last steady state towards a steady state with minimal entropy production (minimal Joule heating) [18].

While in films the mixed state consists of metallic filaments embedded in the semiconductor [19], in single crystals it consists of metallic and semiconducting domains with boundaries crossing the widths of the samples in favorable inclinations [20]. It was recently shown that in contrast to thin-film channels in Mott-FETs, single-crystalline nanowires have superior sensitivity for transport modulation, resulting in ten-fold higher resistance range; this is attributed to the coexisting I–M states in the crystalline channel [21]. VO_2 single crystals or free-standing, crystalline nano-wires have an additional, unique property: in the mixed M–I state: narrow semiconducting domains slide along a metallic background, in the positive sense of the electric current [22–25] being accompanied by relaxation oscillations [24, 26]. This phenomenon has not yet found its use in applications but this may change in the future following progress in the fabrication of free standing nanowires. The sliding domains are very sensitive to the integrity of the crystals; repeated I → M switching cycles or steep switching under low R_L may cause the disappearance of sliding domains without having a significant effect on the ohmic properties of the samples. An example of the high sensitivity of sliding domains to switching is seen in figure 1 of [20]. Semiconducting domains sliding along a metallic background in sample D1(1) are observed at currents above switching during the first three I–V cycles (see loops 2 and 3 and images snipped from a video during the second cycle); their presence is accompanied by a linear increase of the power $P(=IV)$ as function of current. Sliding domains are absent along loop 4 and their absence is accompanied by flattening of $P(I)$. After repeated switching cycles, accumulated damage causes deterioration of all the properties of the samples. Upon switching between steady states in the NDR regime, the power $P = IV$ passes through a maximum (P_{max}) that is steeper the lower R_L is. Thus, steep, damaging switching is prevented in VO_2 single crystals connected to large enough load resistances.

The threshold voltage V_{max} at the onset of NDR regime may be estimated by equating the Joule power with Newton's law of cooling i.e. $P = V^2/R = \alpha \Delta T$, where ΔT is the excess above ambient temperature $T - T_0$, and α is an effective coefficient. R is approximated by the activated resistance as $R = R_0 \cdot \exp(-\Delta T/T_1)$ where R_0 is the resistance at ambient temperature, and T_1 a fitting parameter [27].

$$R(T) = R(T_0 + \Delta T) = R_0 \exp\left[\frac{E_a}{kT} - \frac{E_a}{kT_0}\right] \approx R_0 \exp\left[-\frac{T}{T_1}\right] \tag{1}$$
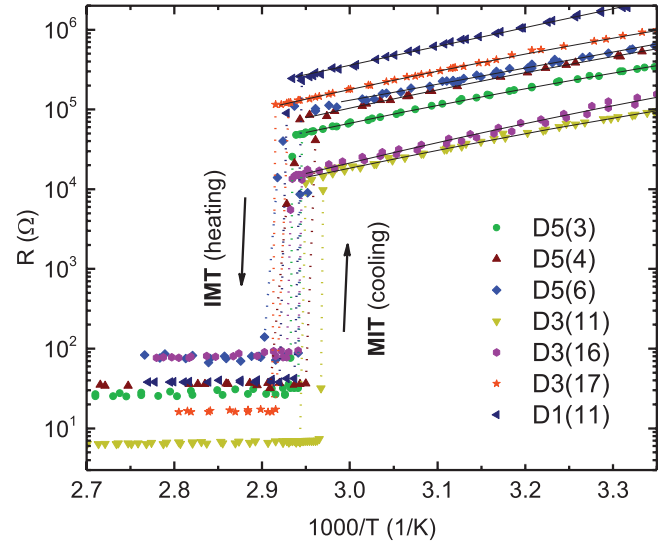

Figure 1. Two-contact resistance: R versus 1000/T for crystals D5(3), D5(4), D5(6), D3(11), D3(16), D3(17) and D1(11).

where $\Delta T = T - T_0$ and the parameter $T_1 = kT_0 \langle T \rangle / E_a$.

This is allowed by the narrow temperature range between room temperature and T_{IMT} (e.g. figure 1). For single crystals with activation energies of $0.4 \leqslant E_a \leqslant 0.5$ eV, this parameter is: $22 \geqslant T_1 \geqslant 17$ K. These approximations lead to $IV = T_1 \ln\left(\frac{IR_0}{V}\right)$ from which the differential resistance dV/dI is derived:

$$\frac{dV}{dI} = \frac{V}{I}\frac{(\alpha T_1 - IV)}{(\alpha T_1 + IV)} = \frac{V}{I}\frac{\left(\frac{T_1}{T} - 1\right)}{\left(\frac{T_1}{T} + 1\right)}. \tag{2}$$

The onset of CC-NDR occurs when $dV/dI = 0$. At this point on the I–V characteristic $T_1 = \Delta T$ (independent of α, [27]). This yields:

$$R = \frac{V}{I} = R_o e^{-1} \tag{3}$$

$$V_{max} = \sqrt{R_o e^{-1} T_1}. \tag{4}$$

The high current limit of the NDR regime $\frac{dV}{dI} = -\frac{V}{I}$ cannot be reached in the insulating state since the onset of the mixed state sets on at finite $\Delta T = T_{IMT} - T_0$.

$|dV/dI|_{max}$ in the NDR regime (that determines the minimal R_L required for stability) is found by setting: $\frac{d^2V}{dI^2} = \frac{2V^2}{I}\left(\frac{(IV)^2 - 3(T_1)^2}{(\alpha T_1 + IV)^3}\right) = 0$ which leads to:

$$\frac{IV}{\alpha T_1} = \sqrt{3} \quad \text{and}$$

$$|dV/dI|_{max} = e^{-\sqrt{3}}\left|\frac{1 - \sqrt{3}}{1 + \sqrt{3}}\right| R_0 = 0.047\,41 R_0. \tag{5}$$

Equations (4) and (5) show that upon decreasing R_0 the maximal voltage on the sample (at the onset of NDR) is reduced and even more important, the load resistance (the main consumer of the applied voltage at high currents) can be reduced. The solution suggested in [20] for reducing R_0 while preserving the quality of VO_2 and its IMT would be to raise the ambient temperature around the functioning VO_2 device.

J. Phys. D: Appl. Phys. **52** (2019) 385302

B Fisher *et al*

Table 1. Properties of the samples used in this work. Length (L), resistivity (ρ) at 300 K, activation energy (E_a), transition temperature upon heating (T_{IMT}) and upon cooling (T_{MIT}), extracted from figure 1. $V_{max}/R_0^{0.5}$ and R^2 represent the slopes in figure 5(a) and their fitting quality, respectively.

Sample	L (cm)	a (cm)	b (cm)	ρ (300 K) (Ω cm)	E_a (eV)	T_{IMT} (K)	T_{MIT} (K)	Surface area (cm²)	$V_{max}/R_0^{1/2}$ (W$^{1/2}$)	R^2
D5(3)	0.15	0.007 36	0.004 85	85	0.412	340.5	339.5	0.003 66	0.0573	0.963
D3(11)	0.15	0.0210	0.0160	199	0.409	339	337	0.0111	0.0928	0.924
D5(4)	0.15	0.0144	0.0049	240	0.414	341	338	0.0058	0.0562	0.905
D3(16)	0.42	0.0260	0.0246	194	0.476	341	339.5	0.0425	0.1202	0.922
D3(17)	0.43	0.0088	0.0044	242	0.429	343	341	0.011 36	0.0926	0.803
D5(6)	0.15	0.0077	0.0060	177	0.400	342	338	0.004 11	0.0553	0.990
D1(11)	0.13	0.0042	0.0020	128	0.467	341.5	340	0.001 61	0.0442	—

There may be another reason for increasing the ambient temperature of the VO$_2$ device close to T_{IMT}: when current is applied on the device at high temperature the I–M transition occurs at a low voltage that has no direct effect on the crystal except of heating. The high voltage needed to induce the transition in the more resistive device at low temperature may affect the lattice causing permanent alterations. The consequences of high voltages applied at low temperatures was shown to have dramatic effects in thin films [14].

Finding optimal conditions for obtaining maximal resistance modulation under steady state conditions and minimal external voltage applied on single crystals is the main objective of this work. In addition, this work provides a test-bed of the simple model of 'Joule heating in VO$_2$ single crystals' derived above.

2. Experimental

Single crystals of VO$_2$ have been grown by self-flux-evaporation [22] from 99.99% V$_2$O$_5$ powder (Sigma Aldrich). Free-standing needle-like shaped crystals have been used in this work (table 1). $R(T)$ of the VO$_2$ crystals was measured in the two-probe configuration (with connected adjacent voltage and current probes) using indium-amalgam dots for contacts. These form Ohmic contacts of low resistance for insulating (semiconducting) VO$_2$. With these contacts, the samples are free to move, being held only by surface tension. I–V measurements were carried out at ambient temperature in the two-probe configuration by varying the applied voltage and the load resistance. The I–V loops were recorded on a YEW type 3036 *X-Y* recorder while the samples were viewed under the microscope. The video clip shown in the supplementary material (stacks. iop.org/JPhysD/52/385302/mmedia) was taken with a smart phone camera mounted on a Zeiss stereo microscope.

3. Results and discussion

Here, we report on the investigation of the effects of the ambient temperatures and of R_L (=101 kΩ, 11 kΩ and 1 kΩ) on the I–V characteristics of two single crystals of VO$_2$ (labelled D5(3), and D3(11), table 1). The results emphasize the striking difference between I–M switching under steady state ($R_L > |dV/dI|_{max}$) and non-steady state ($R_L < |dV/dI|_{max}$) conditions. The I–V characteristics of four more samples,

D5(4), D3(16) and D3(17) were also measured at different ambient temperatures but only for $R_L > |dV/dI|_{max}$ in the NDR regime. $I(V)$, $R(V) = V/I$ and $P(I) = IV(I)$ for samples D5(3) and D5(4) connected to different R_L are presented in the main text, whereas those for D3(11), D3(16), D3(17) and D5(6) are shown in the supplementary material. A smooth transition from insulating to mixed metal-insulator state followed closely by appearance of sliding domains is exhibited by a thin VO$_2$ single crystal—D1(11) examined under the microscope during the I–V cycling under steady state conditions. $V(I)$, $P(I)$ and $u(J)$ (u-sliding velocity, J-current density) for this sample are shown in the main text and two corresponding video clips are shown in the supplementary material. Concluding results derived from all the traces in the main text and in the supplementary material are shown in the main text.

The semilog plots of $R(1/T)$ for the six samples, measured by two contacts—four probes are shown in figure 1. The dimensions of the samples, their specific resistivity ρ at 300 K, the activation energy in the semiconducting state, the transition temperatures upon heating T_{IMT} and upon cooling T_{MIT} obtained from the traces in figure 1 are summarized in table 1. The resistance jumps are limited by the finite contact resistance in the metallic state (between ~7 Ω for D3(11) up to ~80 Ω for D3(16)). For all samples, the transition is very steep and the hysteresis ranges between 1 K for D5(3) to 4 K for D5(6)—an indication of their high crystalline quality. The I–V characteristics of D5(3) at 295 K, 310 K and 320 K, $R(V) = V/I$ and $P(I) = IV$ calculated from the $I(V)$ data are shown in the first column of frames of figure 2 for $R_L = 101$ kΩ, in the second row for $R_L = 11$ kΩ and in the third for $R_L = 1$ kΩ (1 kΩ is the resistor used for the current measurements). In the first row, for the largest R_L, the I–V characteristics show the onset of CC-NDR at V_{max} that decreases as the temperature is increased. Small voltage drops at a current which is independent of T_0 towards a reversible $I(V)$ range mark the onset of the mixed state with the appearance of the first metallic domain (e.g. at ~20 V for 295 K, figure 2(a)). The range of currents in (a) is limited by the large R_L that carries most of the finite source voltage of 200 V. The hysteresis is narrow and the backward transitions occur at slightly lower currents. $R(V)$ calculated from $I(V)$ and $|dV/dI|(V)$ from fitted cubic or higher order polynomials to $V(I)$ in the NDR regime are shown in figure 2(b); the latter are shown below the $R(V)$ curves. For all three
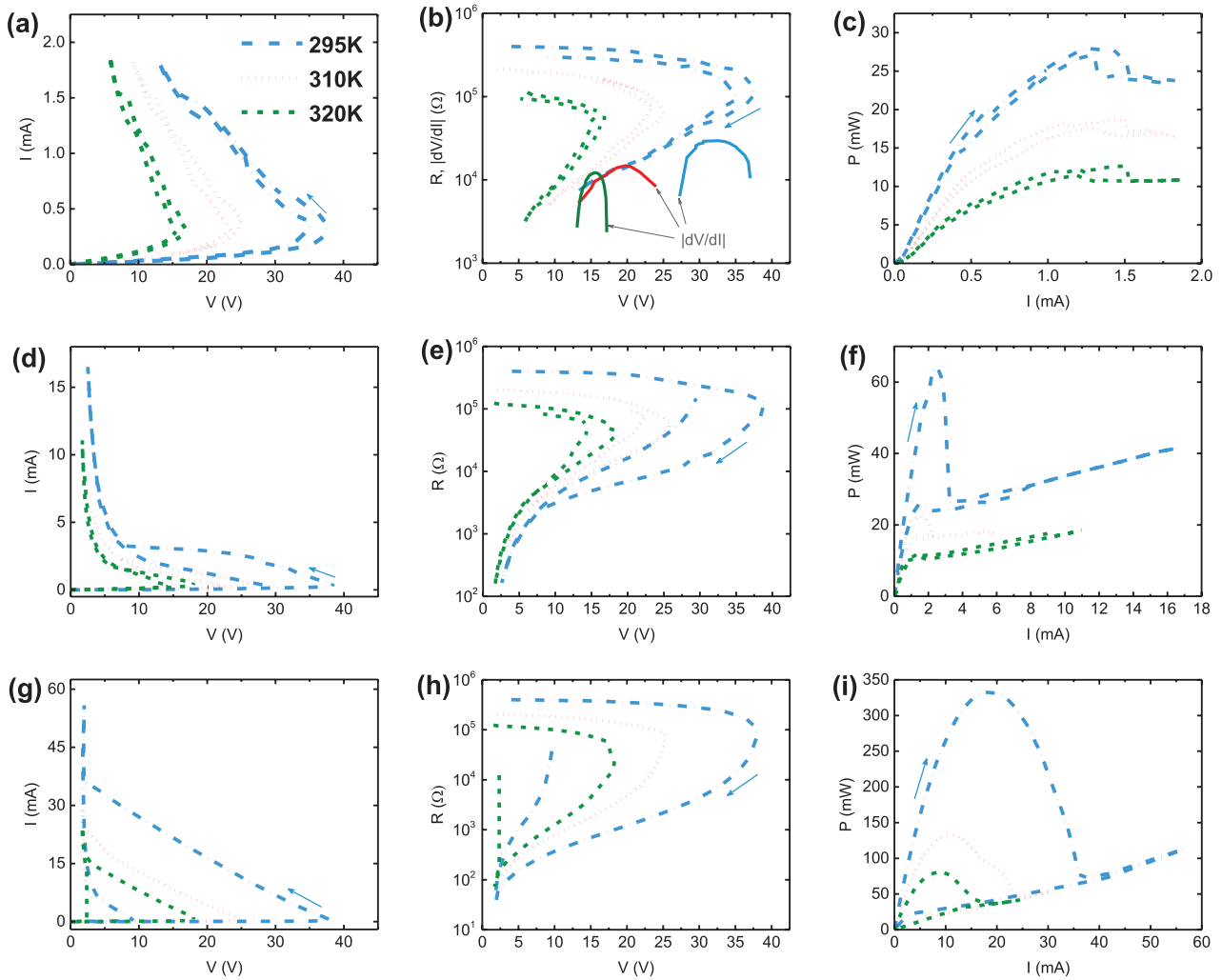
J. Phys. D: Appl. Phys. **52** (2019) 385302

B Fisher *et al*

Figure 2. $I(V)$, $R(V)(=V/I)$ and $P(V)(=VI)$ for sample D5(3) at temperatures 295, 310 and 320 K (see legend in (a)) with $R_L = 101$ kΩ (a)–(c), $R_L = 11$ kΩ (d)–(f) and $R_L = 1$ kΩ (g)–(i). $|dV/dI|(V)$ in the NDR regime is shown in (b) below $R(V)$. Arrows indicate the scan direction.

ambient temperatures, $|dV/dI|_{max} < 101$ kΩ but > 11 kΩ. Thus, the data in the NDR regime with $R_L = 101$ kΩ were obtained under stable conditions while all others, under unstable conditions. Figure 2(c) shows the increase of $P = IV$ with increasing current (increasing temperature) followed by a small but steep decrease as the first metallic domain appears in the sample, at a 1.3–1.5 mA range for all three temperatures. This is consistent with the decrease in infrared emission of metallic VO$_2$ relative to semiconducting VO$_2$ [28, 29].

The range of currents in figure 2(d) is one order of magnitude larger for $R_L = 11$ kΩ compared to 101 kΩ. Switching occurs along a broken line that is steeper close to V_{max} and almost flat before the onset of the reversible (stable) regime. A straight line of slope $\sim 1/R_L$ connects the point at V_{max} with that at the onset of the reversible state. $I(V)$, $R(V)$ and $P(V)$ exhibit large hystereses between forward and backward switching. The lowest resistance reached upon increasing current (figure 2(e)) is still at a safe distance above that of the contact resistance (< 0.1 kΩ, figure 1). P_{max} for $R_L = 11$ kΩ (figure 2(f)) is more than twice larger than for $R_L = 101$ kΩ at 295 K;

interestingly, P_{min} is close to that for the large R_L. The drop of P_{max} with increasing temperature is dramatic. In the reversible (stable) regime, P increases linearly with I. This was quite surprising at the time when it was naively assumed that for fixed temperature (T_{IMT}) P should either be constant or decrease with current due to the increasing fraction of the metallic phase in the mixed state [28]. It was previously shown that the increasing $P(I)$ is correlated to the dynamic phenomena of creation and annihilation of moving M–I domain boundaries. The slope $dp/dj = L^{-1}dP/Di \approx 8$ V cm^{-1} for this sample (p-power density, j-current density and L-sample's length) falls within the range of such phenomena observed in [20].

The range of currents for $R_L = 1$ kΩ was intentionally limited to only a factor of ~ 3 relative to the previous case, so that the lowest resistance would not reach the contact resistance. Switching in figure 2(g) is along a straight line of slope $\sim 1/R_L$ from the onset of NDR to the reversible (stable) range of currents. The hystereses in all graphs of the three frames are huge. At 295 K, P_{max} for 1 kΩ is larger than P_{max} for 101 kΩ by more than an order of magnitude (figure 2(i)).
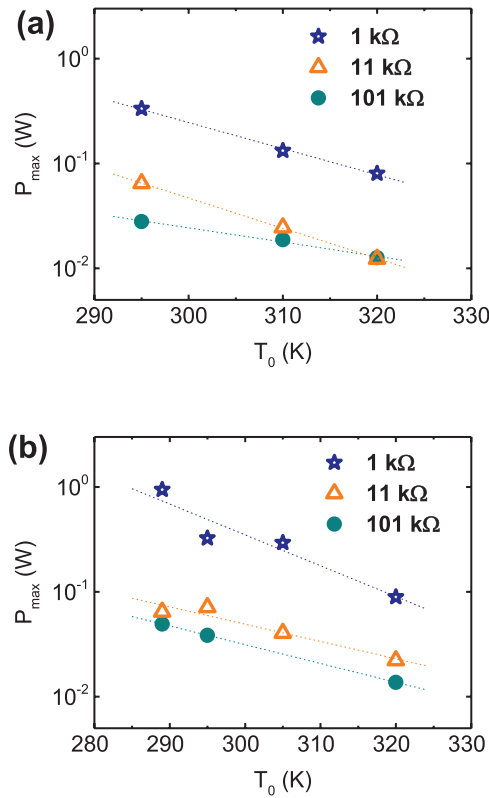
(a)

(b)

Figure 3. The peak power P_{max} at switching versus ambient temperature T_0 for crystals D5(3) (a) and D3(11) (b) connected to the different load resistances R_L.

The effect of R_L on P_{max} is revealed in figure 3(a) for sample D5(3) and in 3(b) for D3(11) (figure S3, supplementary material). Semilog $P_{max}(T_0)$ representation was chosen in order to provide equal weights to the data that are spread over almost two orders of magnitude.

In figure 3(a), the fitted lines for $R_L = 1\,k\Omega$ and $R_L = 11\,k\Omega$ have relatively higher slopes and below them lies the line for $R_L = 101\,k\Omega$ with a much lower slope. In figure 3(b), the line at the top (for $R_L = 1\,k\Omega$) has a high slope while the two at the bottom (for $R_L = 11\,k\Omega$ and $R_L = 101\,k\Omega$) have relatively lower slopes. The data on the lines with high slopes were obtained under non-steady state conditions (i.e. $R_L < |dV/dI|_{max}$ for the respective characteristic). With one exception, the data on the lines with low slopes were obtained under steady state conditions. The exception is the datum point for D3(11) at 289 K (see figure S3 in the supplementary material). It represents the I–V characteristic that deviates from the 'well behaved' form in figure S3(f) and shows that this characteristic is for a non-steady state. In fact, a line for $R_L = 11\,k\Omega$ fitted to the three data points for the higher temperatures would be parallel to the line for $R_L = 101\,k\Omega$. According to our simple model $P_{max} \propto (T_{IMT} - T_0)$; for narrow ranges the exponential function is close to linear. Therefore, the overall behavior in figure 3 agrees with our proposed model where $P \propto \Delta T$ in steady state.

I–V measurements on sample D5(4) (figure 4) were devoted to finding the optimal, steady state conditions for insulator—mixed metal-insulator transition induced by current, that is, maximal resistance modulation for minimal applied voltage.

Steady state implies removal of the damaging bell shaped $P(I)$ in the NDR regime (e.g. figure 2(f) and (i)).

The I–V characteristics, $R(V)$ and $P(I)$ for $R_L = 101\,k\Omega$ are shown in figures 4((a)–(c)) for sample D5(4). The traces of $|dV/dI|(V)$ for this large R_L are shown below the $R(V)$ traces in figure 4(b). They show that $|dV/dI|_{max} = 26.1\,k\Omega$, $25.0\,k\Omega$ and $24.6\,k\Omega$ for $T_0 = 295\,K$, $307\,K$ and $320\,K$, respectively. These traces for $R_L = 34\,k\Omega$ (out of caution, not the lowest possible R_L) are shown in figures 4((d)–(f)). The range of currents was increased by a factor of three and that of the resistance modulation by one order of magnitude. The lowest resistance in 4(e) is more than one order of magnitude higher than the contact resistance. The results in figure 4(f) are in strong contrast with those shown in figures 2(f) and (i) for sample D5(3) (and those of figure S3(i) for sample D3(11)). For all three temperatures $P(I)$ reaches shallow maxima followed by shallow dips associated with the appearance of metallic domains. After a range where $P(I)$ shows a rather noisy behavior, reversible ranges are reached. The widest range of currents over which $P(I)$ is reversible is obtained for $T_0 = 320\,K$. The slope of this trace in the reversible regime is $dP/dI \approx 1.5$ V (comparable to that in figure 2(f)) and corresponds to $dp/dj = 10$ V cm^{-1}. The low V_{max} and the wide reversible regime emphasize the advantage of working at $T_0 = 320\,K$. In other words, at low resistance it is distinctly adventitious to perform current-induced switching of VO$_2$ intuitively be expressed as switching in the conditions where crystals are close to their IMT temperature. This results in less driving force, which promotes a 'clean' transition that yields reversible, damage-free behavior.

In figure 5, we compare results obtained for the six samples by which the validity of the simple model of 'Joule heating' is examined.

In figure 5(a), we plotted V_{max} versus $R_0^{1/2}$ according to the model's predictions (equation (4)). The heights of the symbols in figure 5 exceed the experimental uncertainties in V_{max} and in $|dV/dI|_{max}$, respectively. The uncertainties along the horizontal axis are attributed to deviations in R_0 caused by small deviations in T_0 (~0.5 K). In principle, for a given sample V_{max} should depend only on temperature and not on the load resistance. This holds for all but sample D3(11) at 295 K. The slopes of the lines and the respective quality of fit are summarized in the last two columns of in table 1. The values of R^2 (>0.9) for all but that for sample D3(17) (=0.8) indicate fairly good agreement between the experimental results and predictions. The fitted lines for D3(11) and D3(17) almost coincide and so do the three fitted lines for D5(3), D5(4) and D5(6). The surface areas of the first pair of samples is incidentally identical (table 1), those for the other three are close but a small uncertainty in their small dimensions could account for the difference between their areas. The correlation between V_{max}^2/R_0 and surface areas found for these five samples stresses the fact that the heat dissipation is almost exclusively from the surface of the samples, and therefore heat conduction through the contacts is insignificant.

The $|dV/dI|_{max}$ data versus R_0 obtained from the $V(I)$ traces for the six samples in the stable states of NDR are plotted in figure 5(b). The data points are best fit by the line
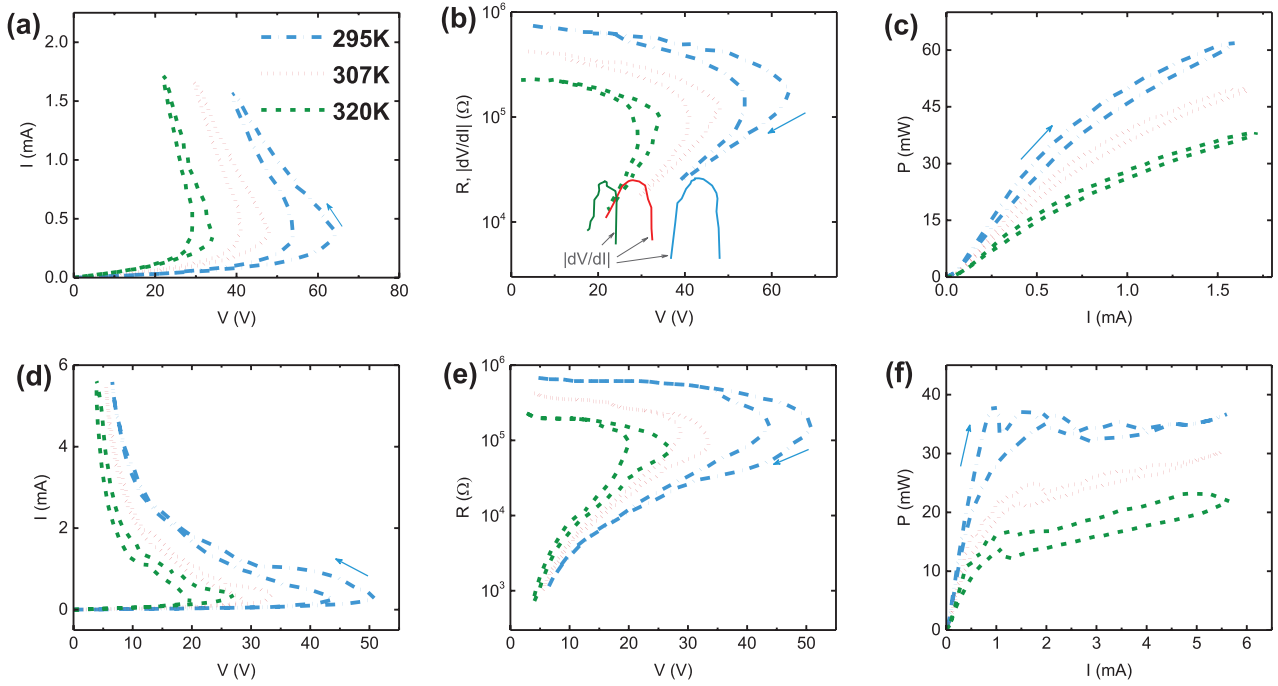
Figure 4. $I(V)$, $R(V)(=V/I)$ and $P(V)(=VI)$ for sample D5(4) at temperatures 295 K, 307 K and 320 K (see legend in (a)) with $R_L = 101$ kΩ (a)–(c) and $R_L = 34$ kΩ (d)–(f). $|dV/dI|(V)$ in the NDR regime is shown in (b) below $R(V)$. Arrows indicate the scan direction.
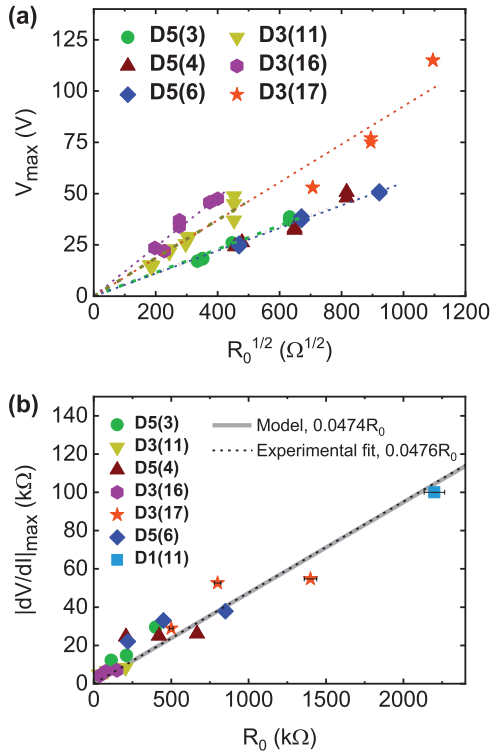

Figure 5. (a) V_{max} versus $R_0^{1/2}$ for crystals D5(3), D3(11), D5(4), D5(6), D3(16) and D3(17). (b) $|dV/dI|_{max}$ versus R_0. The experimental uncertainty is smaller than the size of the data points, unless otherwise noted.

$|dV/dI|_{max} = 0.0476\, R_0$, ($R^2 = 0.883$). The model predicts $|dV/dI|_{max} = 0.0474\, R_0$ (equation (5)) for NDR in the insulating state. The onset of the mixed M–I state changes the slope of dV/dI from that derived for the insulating state. For $T_0 = 320$ K (with T_1 around 20 K) the onset of NDR (at $T_0 + T_1$) and of the mixed state at T_{IMT} are very close. Therefore, to warrant steady state $|dV/dI|_{max}$ should be determined experimentally for each device at each ambient temperature. In a more general case, for applied AC, the load resistance R_L should be replaced by the load impedance, Z_L.

$V(I)$ and $P(I)$ for the very thin sample D1(11) examined under the microscope during *I–V* cycling are shown in figures 6(a) and (b) under steady state conditions ($R_L = 500$ kΩ). The temperature measured by a thermocouple close to the sample was 300 K (slightly larger than RT due to the constant illumination of the sample). The most impressive result here is the smooth insulator to mixed-metal-insulator transition exhibited by the bending of the $P(I)$ curve. The bending is followed closely by the appearance of sliding semiconducting domains within the metallic background in the sense of the electric current. In the mixed state $dP/dI = 28$ V and corresponds to $dp/dj = 215$ V cm^{-1}, far larger than the corresponding values obtained in the thicker samples. The symbols on $I(V)$ and $P(I)$ mark the points where the sliding domains were recorded on video. The full circles mark two video clips recorded at different currents attached to the supplementary material. The sliding velocity (u) as function of current density (J) are shown in figure 6(c). The fitted $u/J = 0.00057$ cm^3
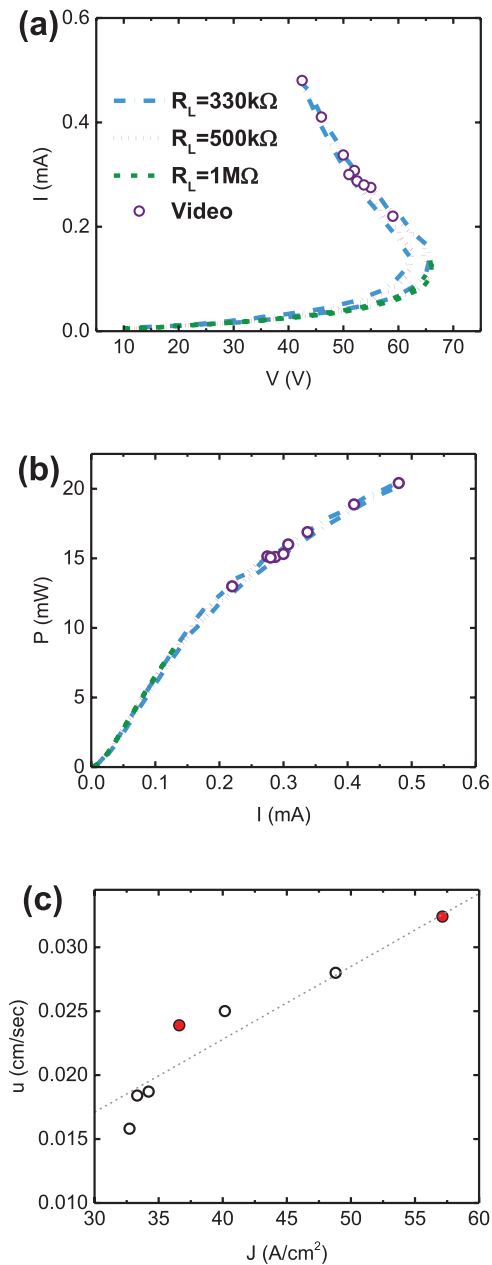
J. Phys. D: Appl. Phys. **52** (2019) 385302

B Fisher *et al*

Figure 6. *I(V)* (a) *P(I)* (b) and sliding velocity of domains u as function of current density *J* (c) at 300 K. Red circles in (c) refer to the video clips attached to the supplementary material.

As^{-1} ($R^2 = 0.89$) is about ½ the maximal value obtained in VO$_2$ single crystals and is comparable to the value obtained in a sample labeled D2(9) (figure 7 in [16]). As in the case of D2(9), the low *u/J* value obtained for D1(11) may be attributed to its poor morphology.

4. Conclusion

In conclusion, our *I–V* measurements show the advantage of increasing the ambient temperature around single-crystalline devices avoiding steep switching by maintaining steady state in the NDR regime while reducing power consumption. Since the main problem in electronics is cooling the devices, the increase of ambient temperature relative to room temperature

means less cooling, an additional contribution to reduction in power consumption.

The results indicate that the simple 'Joule heating model', though not rigorous, is very useful for orientation within the various regimes of the *I–V* characteristics. Large deviations of the measured |d*V*/d*I*|$_{max}$, calculated from the model (derived for the insulating regime) are caused by the appearance of the mixed I–M state within the NDR regime.

Supplementary material

See supplementary material for two graphs supporting the simple model of 'Joule heating in VO$_2$ single crystals', graphs of the full electrical analysis of samples D5(6), D3(11), D3(16) and D3(17) and for sliding domains recorded on videos.

ORCID iDs

Lior Kornblum https://orcid.org/0000-0001-6305-7619

References

[1] Liu K, Lee S, Yang S, Delaire O and Wu J 2018 Recent progresses on physics and applications of vanadium dioxide *Mater. Today* **21** 875–96
[2] Kim H-T *et al* 2004 Mechanism and observation of Mott transition in VO$_2$-based two- and three-terminal devices *New J. Phys.* **6** 52
[3] Zhou Y, Chen X, Ko C, Yang Z, Mouli C and Ramanathan S 2013 Voltage-triggered ultrafast phase transition in vanadium dioxide switches *IEEE Electron Device Lett.* **34** 220–2
[4] Zhou Y and Ramanathan S 2013 Correlated electron materials and field effect transistors for logic: a review *Crit. Rev. Solid State Mater. Sci.* **38** 286–317
[5] Shukla N *et al* 2015 A steep-slope transistor based on abrupt electronic phase transition *Nat. Commun.* **6** 7812
[6] Madan H *et al* 2015 26.5 Terahertz electrically triggered RF switch on epitaxial VO$_2$-on-sapphire (VOS) wafer *2015 IEEE Int. Electron Devices Meeting* pp 9.3.1–4
[7] Vitale W A *et al* 2017 A steep-slope transistor combining phase-change and band-to-band-tunneling to achieve a sub-unity body factor *Sci. Rep.* **7** 355
[8] Abreu E *et al* 2017 Ultrafast electron-lattice coupling dynamics in VO$_2$ V$_2$O$_3$ thin films *Phys. Rev.* B **96** 094309
[9] Liu Z *et al* 2018 Dynamic infrared thin-film absorbers with tunable absorption level based on VO$_2$ phase transition *Opt. Mater. Express* **8** 2151–8
[10] Casu E A *et al* 2018 Vanadium oxide bandstop tunable filter for Ka frequency bands based on a novel reconfigurable spiral shape defected ground plane CPW *IEEE Access* **6** 12206–12
[11] Verma A *et al* 2018 Steep sub-Boltzmann switching in AlGaN/ GaN phase-FETs with ALD VO$_2$ *IEEE Trans. Electron Devices* **65** 945–9

[12] del Valle J, Ramírez J G, Rozenberg M J and Schuller I K 2018 Challenges in materials and devices for resistive-switching-based neuromorphic computing *J. Appl. Phys.* **124** 211101

[13] Lee D *et al* 2018 Isostructural metal-insulator transition in VO$_2$ *Science* **362** 1037–40

[14] del Valle J, Kalcheim Y, Trastoy J, Charnukha A, Basov D N and Schuller I K 2017 Electrically induced multiple metal–insulator transitions in oxide nanodevices *Phys. Rev. Appl.* **8** 054041

[15] Lee S *et al* 2017 Anomalously low electronic thermal conductivity in metallic vanadium dioxide *Science* **355** 371–4

[16] Fisher B and Patlagan L 2017 Switching VO$_2$ single crystals and related phenomena: sliding domains and crack formation *Materials* **10** 554

[17] Beneking H and Beneking B 1994 *High Speed Semiconductor Devices: Circuit Aspects and Fundamental Behaviour* (Berlin: Springer)

[18] Ridley B K 1963 Specific negative resistance in solids *Proc. Phys. Soc.* **82** 954

[19] Li D *et al* 2016 Joule heating-induced metal–insulator transition in epitaxial VO$_2$/TiO$_2$ devices *ACS Appl. Mater. Interfaces* **8** 12908–14

[20] Fisher B and Patlagan L 2018 Power dissipation in the mixed metal-insulator state of self-heated VO$_2$ single crystals and the effect of sliding domains *Appl. Phys. Lett.* **112** 231905

[21] Wei T, Kanki T, Chikanari M, Uemura T, Sekitani T and Tanaka H 2017 Enhanced electronic-transport modulation in single-crystalline VO$_2$ nanowire-based solid-state field-effect transistors *Sci. Rep.* **7** 17215

[22] Fisher B 1975 Moving boundaries and travelling domains during switching of VO$_2$ single crystals *J. Phys. C: Solid State Phys.* **8** 2072

[23] Fisher B 1976 Metal-semiconductor domain configurations during switching of VO$_2$ single crystals *J. Phys. C: Solid State Phys.* **9** 1201

[24] Gu Q, Falk A, Wu J, Ouyang L and Park H 2007 Current-driven phase oscillation and domain-wall propagation in W$_x$V$_{1-x}$O$_2$ nanobeams *Nano Lett.* **7** 363–6

[25] Tselev A, Budai J D, Strelcov E, Tischler J Z, Kolmakov A and Kalinin S V 2011 Electromechanical actuation and current-induced metastable states in suspended single-crystalline VO$_2$ nanoplatelets *Nano Lett.* **11** 3065–73

[26] Fisher B 1978 Voltage oscillations in switching VO$_2$ needles *J. Appl. Phys.* **49** 5339–41

[27] Fisher B, Genossar J, Patlagan L and Reisner G M 2013 Electric-field effects in resistive oxides: facts and artifacts *EPJ Web Conf.* **40** 15009

[28] Kats M A *et al* 2013 Vanadium dioxide as a natural disordered metamaterial: perfect thermal emission and large broadband negative differential thermal emittance *Phys. Rev.* X **3** 041004

[29] Ramirez-Rincon J A *et al* 2018 Thermal hysteresis measurement of the VO$_2$ dielectric function for its metal-insulator transition by visible-IR ellipsometry *J. Appl. Phys.* **124** 195102